The Henle Fiber Layer in Albinism: Comparison to Normal and Relationship to Outer Nuclear Layer Thickness and Foveal Cone Density

Daniel J. Lee,[1] Erica N. Woertz,[2] Alexis Visotcky,[3] Melissa A. Wilk,[4] Heather Heitkotter,[2] Rachel E. Linderman,[2] Sergey Tarima,[3] C. Gail Summers,[5,6] Brian P. Brooks,[7] Murray H. Brilliant,[8] Bhavna J. Antony,[9] Brandon J. Lujan,[10] and Joseph Carroll[2,11]

[1]Medical College of Wisconsin, Milwaukee, Wisconsin, United States
[2]Cell Biology, Neurobiology & Anatomy, Medical College of Wisconsin, Milwaukee, Wisconsin, United States
[3]Division of Biostatistics, Institute for Health and Equity, Medical College of Wisconsin, Milwaukee, Wisconsin, United States
[4]HudsonAlpha Institute for Biotechnology, Huntsville, Alabama, United States
[5]Department of Ophthalmology & Visual Neurosciences, University of Minnesota, Minneapolis, Minnesota, United States
[6]Department of Pediatrics, University of Minnesota, Minneapolis, Minnesota, United States
[7]National Eye Institute, Bethesda, Maryland, United States
[8]Center for Human Genetics, Marshfield Clinic Research Institute, Marshfield, Wisconsin, United States
[9]IBM Research-Australia, Southbank, Victoria, Australia
[10]Casey Eye Institute, Oregon Health & Science University, Portland, Oregon, United States
[11]Ophthalmology & Visual Sciences, Medical College of Wisconsin, Milwaukee, Wisconsin, United States

Correspondence: Joseph Carroll, Department of Ophthalmology & Visual Sciences, Medical College of Wisconsin, 925 N 87th Street, Milwaukee, WI 53226-0509, USA; jcarroll@mcw.edu.

DJL and ENW contributed equally to the work presented here and should therefore be regarded as equivalent authors.

Submitted: July 20, 2018
Accepted: September 24, 2018

Citation: Lee DJ, Woertz EN, Visotcky A, et al. The Henle fiber layer in albinism: comparison to normal and relationship to outer nuclear layer thickness and foveal cone density. *Invest Ophthalmol Vis Sci*. 2018;59:5336–5348. https://doi.org/10.1167/iovs.18-24145

Purpose. Directional optical coherence tomography (D-OCT) allows the visualization of the Henle fiber layer (HFL) in vivo. Here, we used D-OCT to characterize the HFL and outer nuclear layer (ONL) in albinism and examine the relationship between true foveal ONL and peak cone density.

Methods. Horizontal D-OCT B-scans were acquired, registered, and averaged for 12 subjects with oculocutaneous albinism and 26 control subjects. Averaged images were manually segmented to extract HFL and ONL thickness. Adaptive optics scanning light ophthalmoscopy was used to acquire images of the foveal cone mosaic in 10 subjects with albinism, from which peak cone density was assessed.

Results. Across the foveal region, the HFL topography was different between subjects with albinism and normal controls. In particular, foveal HFL thickness was thicker in albinism than in normal controls ($P < 0.0001$), whereas foveal ONL thickness was thinner in albinism than in normal controls ($P < 0.0001$). The total HFL and ONL thickness was not significantly different between albinism and controls ($P = 0.3169$). Foveal ONL thickness was positively correlated with peak cone density in subjects with albinism ($r = 0.8061$, $P = 0.0072$).

Conclusions. Foveal HFL and ONL topography are significantly altered in albinism relative to normal controls. Our data suggest that increased foveal cone packing drives the formation of Henle fibers, more so than the lateral displacement of inner retinal neurons (which is reduced in albinism). The ability to quantify foveal ONL and HFL may help further stratify grading schemes used to assess foveal hypoplasia.

Keywords: Henle fiber layer, albinism, fovea, outer nuclear layer, optical coherence tomography

The human fovea can be distinguished from the rest of the retina by a lateral displacement of inner retinal neurons, the presence of an avascular zone, lengthening of the photoreceptor outer segments, and increased cone packing density.[1,2] Although the fovea comprises only about 0.1% of the retinal surface area, it underlies a significant portion of our visual function. As such, developmental or acquired disruption of normal foveal architecture can lead to decreased visual function.[3–5] Because of this, there is significant interest in understanding foveal development in health and disease. Previous work relied on histologic data to piece together a picture of the developmental progression of anatomic foveal specializations,[2,6,7] although more recent studies using noninvasive optical coherence tomography (OCT) in infants have been able to monitor foveal development both cross-sectionally and longitudinally in a given eye.[8–11] Although these studies provide valuable information on the process of normal foveal development, infants are a challenging population in which to assess how perturbations in foveal development affect visual function.

Albinism is a heterogeneous disorder associated with "arrested" foveal development, most commonly characterized by foveal hypoplasia.[4,12–14] Albinism (and other conditions associated with altered foveal anatomy) provides a natural model

to explore relationships within and between the various anatomic specializations associated with the fovea. Such data are valuable not only for informing models of foveal development but also for understanding the functional deficits in albinism.[4,15–18] Foveal morphology can vary significantly across subjects with albinism[4,14–16,19] and can even overlap with that seen in individuals with normal vision.[16] As such, the clinical descriptor of foveal hypoplasia is insufficient to fully characterize the "maturity" of a given fovea. To this end, Thomas et al.[4] proposed a qualitative grading scheme for assessing the degree of foveal hypoplasia in albinism and other disorders using OCT. Their structure-based system resulted in four grades of foveal hypoplasia, based on the presence or absence of (1) inner retinal neuron extrusion, (2) a foveal pit, (3) outer segment lengthening, and (4) outer nuclear layer (ONL) widening (referring to the increased ONL thickness present at the fovea relative to the parafovea). As OCT is an inherently quantitative imaging modality, we have an interest in exploring the modification of this and other grading schemes by leveraging quantitative information from in vivo retinal imagery.

Quantifying ONL thickness using OCT provides a convenient and noninvasive measure to assess photoreceptor structure. Measures of ONL thickness are routinely used to characterize retinal health in a wide range of inherited retinal degenerations.[20–23] Of particular interest is foveal ONL thickness, again, due to the importance of the fovea for our visual function. The fovea contains nearly exclusively cone photoreceptors, and the density of cone photoreceptors can be directly assessed using adaptive optics (AO) imaging tools.[16,18,24–27] As AO images visualize photoreceptor inner and/or outer segments, while the ONL is comprised of photoreceptor cell bodies, they provide complementary information about photoreceptor structure. This is consistent with outer segment length and ONL thickness being considered as independent factors in the foveal hypoplasia grading scheme mentioned above.[4] In addition, the relationship between cone density and ONL thickness is of significant interest in studying retinal degenerations, as photoreceptors are thought to degenerate in a progressive fashion, with the outer and inner segments degenerating before the nuclei.[28–30] However, a major challenge in assessing this relationship with in vivo imaging is the contamination of ONL thickness by the Henle fiber layer (HFL) in conventional OCT images.[31,32]

Even though the HFL can contribute to more than half of the retinal thickness between the external limiting membrane layer (ELM) and the outer plexiform layer (OPL) on histology,[31,33] the HFL is commonly (and erroneously) characterized as part of the ONL thickness on OCT imaging.[22,34–37] Although it can be challenging to differentiate the HFL from the adjacent ONL on conventional OCT, directional OCT (D-OCT) is an imaging technique that allows for a clear delineation of the HFL from the adjacent ONL by purposefully altering the OCT beam entry position and taking advantage of the Henle fiber's oblique orientation and unique reflective properties.[31,32,38] Here, we used D-OCT to measure the HFL in subjects with albinism. Our primary objectives in the present study were to compare HFL and ONL thickness between albinism and normal subjects and to examine the relationship between ONL and cone density in albinism.

Methods

Subjects

This study followed the tenets of the Declaration of Helsinki and was approved by the Medical College of Wisconsin Institutional Review Board (protocol PRO23898). Informed consent was obtained from all subjects or from an appropriate adult guardian in the case of minors, after explaining the nature and possible consequences of the study. Twelve subjects with oculocutaneous albinism and 26 normal control subjects with no known ocular pathology were recruited to participate in this study. Prior to imaging, subjects were given one drop of phenylephrine hydrochloride (2.5%) followed by one drop of tropicamide (1%) to both eyes to dilate the pupil and suspend accommodation. Minors were given cyclopentolate (1%) in place of tropicamide (1%). An IOL Master (Carl Zeiss Meditec, Dublin, CA, USA) was used to measure axial length to correct for the lateral scale of all retinal images, as previously described.[16]

Genetic Testing

Genotypes for all subjects with albinism were determined by genetic testing, as previously described.[16] Results were evaluated for mutations in the *TYR*, *OCA2*, *TYRP1*, *SLC45A2*, *SLC24A5* (oculocutaneous albinism type 1 [OCA1], OC2, OCA3, OCA4, and OCA6, respectively), and/or *GPR143* (OA1) genes. Identified mutations were compared to the Albinism Database (available in the public domain at http://albinismdb.med.umn.edu/) and additional review of published literature to determine novelty. The predicted protein sequence for a novel frameshift mutation was determined using ExPASy (available in the public domain at https://web.expasy.org/translate/, accessed February 2018).

OCT Imaging

Fourteen eyes of 12 subjects diagnosed with oculocutaneous albinism and 39 eyes of 26 subjects with no known ocular pathology were imaged using a single Cirrus HD-OCT device (Carl Zeiss Meditec). A total of three horizontal scans, one central "flat" scan and two off-axis "tilted" scans, were obtained per eye by using the central line of the high definition 5-line raster setting, which used an average of 20 B-scans per line scan (1024 A-scans/B-scan). In normal controls, the central scan was defined as the scan obtained with central pupil entry position during OCT acquisition.[31,32,38] Because the visual axis is displaced in albinism, the central scan was acquired by imaging the subjects at a pupil entry position slightly off-center from the preferred retinal locus of fixation (Fig. 1). Volumetric images (nominally 6×6 mm; 512 A-scans/B-scan, 128 B-scans) were also acquired (using central pupil entry) for each subject to assess the position of the line scans relative to the foveal pit.

Measuring HFL and ONL Thickness From D-OCT Scans

Each subject's two off-axis B-scans were registered to their central scan by means of identification of similar points of agreement between the images by using custom MATLAB software (Mathworks, Natick, MA, USA).[38,39] Subsequently, the registered D-OCT image sets were stacked on top of one another to verify alignment of the images using ImageJ (National Institutes of Health, Bethesda, MD, USA).[40] Registration was considered acceptable if there was minimal movement (subjectively assessed by a single grader, DJL) of either the internal limiting membrane (ILM) contour, the retinal pigment epithelium contour, and the choroidal vessels (Supplementary Video S1, S2). Only images from one eye per subject were used for subsequent image analysis. In subjects where both eyes were imaged, the D-OCT image set of the eye with better registration and alignment was used for analysis. Left eyes were horizontally flipped to be right eye equivalents for purposes of nasal and temporal comparisons across subjects.

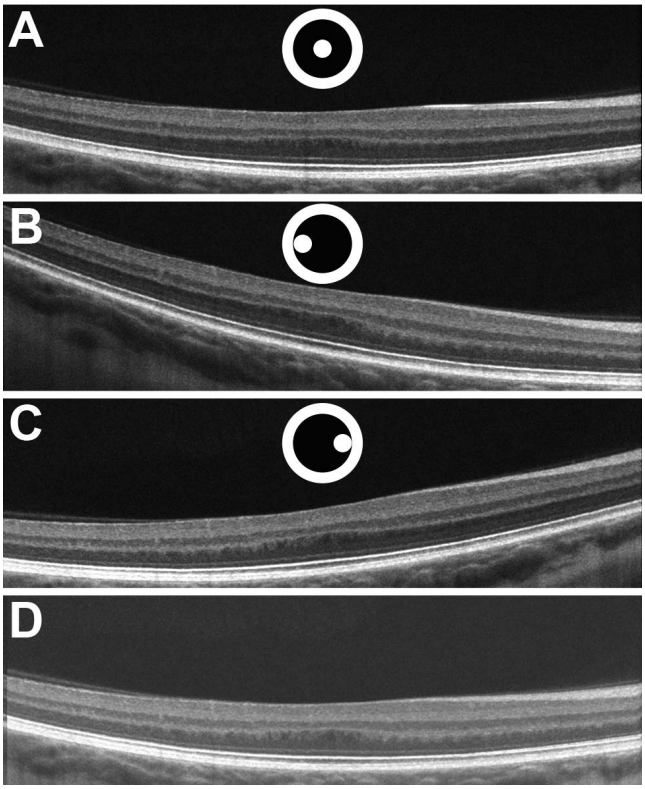

FIGURE 1. D-OCT imaging adequately reveals HFL in subjects with albinism by altering pupil entry position during OCT imaging. One central scan (**A**) and two off-axis scans (**B, C**) are acquired, registered, and averaged to obtain the final merged D-OCT image (**D**). The *black circle* in the center is representative of the pupil, and the *white dot* inside of the central circle is representative of the pupil entry position. Although the center of the pupil was used to acquire the central scan in our controls (as depicted by image **A**), it should be noted that the central scan in albinism was acquired by imaging the subjects at a pupil entry position slightly off-center from the preferred retinal locus of fixation due to the large positive angle kappa evident in albinism. The pupil positions depicted in images **B** and **C** are relative to the pupil entry position used to acquire image **A** in subjects with albinism and are not drawn to scale.

Using ImageJ, registered D-OCT image triads for our subjects with albinism and normal controls were manually segmented by three graders of varying familiarity to D-OCT imaging and segmentation (DJL, ENW, HH) to assess for intragrader repeatability and agreement. The three graders manually segmented D-OCT image triads after receiving standardized training on manual segmentation of D-OCT images in normal and diseased retina. It is worth noting that grader 1 (DJL) had the most prior experience in segmentation of D-OCT images, whereas grader 3 (HH) had the least experience. Each grader assessed the set of 38 D-OCT images three times for a total of nine trials per image (342 images total). Boundaries were determined at the ILM, the interface between the OPL and HFL, the interface between HFL and ONL, the ELM, the ellipsoid zone junction, and the interdigitation zone (Fig. 2). During the manual segmentation process, final merged images were stacked with the two aligned tilted scans during the manual segmentation process. This allowed us to use the hyporeflective appearance of the HFL on the tilted scans to carefully delineate the HFL from the overlying OPL on the final merged image (Supplementary Video S1, S2). A total of 180 points was applied to merged images (30 segmentation points per boundary), and layer thickness was

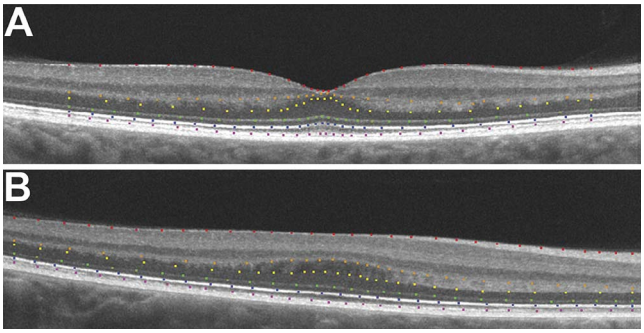

FIGURE 2. Registered D-OCT image triads for a normal control (**A**) and a subject with albinism (**B**) were manually segmented on the final merged image by using ImageJ. Final merged images were stacked with the two aligned tilted scans during the manual segmentation process. This allowed us to use the hyporeflective appearance of the HFL on the tilted scans to carefully delineate the HFL from the overlying OPL on the final merged image (Supplementary Video S1, S2). Boundaries were determined at the ILM (*red*), the OPL/HFL interface (*orange*), the HFL/ONL interface (*yellow*), the ELM (*green*), the ellipsoid zone (*blue*), and the interdigitation zone (*purple*).

then calculated using custom MATLAB software (Mathworks), as previously described.[38] The HFL thickness was obtained by finding the difference between the OPL/HFL and HFL/ONL interface. Similarly, ONL thickness was obtained by calculating the difference between the HFL/ONL interface and the ELM. Thickness measurements were then binned and averaged to a set of common foveal coordinates relative to the foveal center (determined by a single grader, DJL). Area under the curve (AUC) was calculated for the HFL and ONL in each subject by using trapezoidal numerical integration of the binned and averaged thickness measurements.

Assessing Peak Cone Density

For four subjects with albinism, confocal reflectance adaptive optics scanning laser ophthalmoscope (AOSLO) was used to image the foveal cone mosaic, and the images were subsequently registered and montaged as previously described.[41] The peak cone density of each subject was then estimated as previously described.[16] Briefly, a region of the foveal cone mosaic consisting of the area of peak cone density was identified and cropped. Cones in the cropped image were identified using semiautomated software.[42] The density at each pixel in the cropped image was then obtained by counting the cones in variable window sizes. The densities at each pixel for the different window sizes were subsequently averaged, and the pixel with the greatest average density was identified as the location of peak cone density. The peak foveal cone density was recorded using a 37×37-μm sampling window. Previously published peak cone density values were used for six additional subjects with albinism, as noted on Table 1.[16,18]

Statistical Analysis

Statistical analyses were performed using Prism version 7.0c (GraphPad, La Jolla, CA, USA) unless otherwise noted. The D'Agostino and Pearson test was used to assess normality (using $P < 0.05$ as a cutoff) of the various data sets and guide the application of parametric or nonparametric statistical tests as appropriate. Intraclass correlation coefficients (ICCs) were calculated for each grader's foveal HFL+ONL, HFL, and ONL measurements by using R statistical software (Foundation for Statistical Computing, Vienna, Austria). In addition, the intragrader repeatability of foveal HFL+ONL, HFL, and ONL measurements was examined by using the Bland-Altman

Investigative Ophthalmology & Visual Science

Table 1. Subject Demographics for Albinism

Subject Identifier	Age, y	Sex	Eye*	Axial Length, mm	Peak Cone Density, Cones/mm^2	Best-Corrected Visual Acuity, logMAR	Genotype
BB_10965	44	F	OS	24.99	93,500	0.24	*TYR* c.1205G>A; p.R402Q (hom) *SLC24A5* c.1361T>A; p.L454X (hom)
GS_10979	17	M	OD	24.10	71,600	0.08	*TYR* c.1205G>A; p.R402Q (hom) *OCA2* c.913C>T; p.R305W *OCA2* c.1256G>A; p.R419Q
JC_0492†‡	28	F	OD	23.62	81,800	0.10	*TYR* c.1147G>A; p.D383N *TYR* c.1217C>T; p.P406L
JC_0493†‡	21	F	OD	22.33	89,100	0.00	*TYR* c.1147G>A; p.D383N *TYR* c.1217C>T; p.P406L
JC_0829†‡	10	F	OD	21.43	84,700	1.00§	*TYR* c.899A>C; p.300N>T *TYR* c.1217C>T; p.406P>L *TYR* c.1467_1468insT; p.A490Cfr
JC_10227‡	18	F	OD	22.82	78,900	0.32	*OCA2* c.1327G>A; p.V443I
JC_10278‡	14	M	OD	22.82	81,600	0.18	*TYR* c.286_287insA; p.M96Nfr *TYR* c.1205G>A; p.R402Q *TYR* c.575C>A; p.S192Y
JC_10496	69	M	OD	25.87	90,500	0.32	*TYR* c.1205G>A; p.R402Q *OCA2* c.913C>T; p.R305W *OCA2* c.1327G>A; p.V443I *OCA2* c.1465A>G; p.N489D
JC_10508	37	F	OD	22.18	124,100	0.16	*TYR* c.1118C>A; p.T373K *TYR* c.1205G>A; p.R402Q *TYR* c.575C>A; p.S192Y (hom) *OCA2* c.1441G>A; p.A481T
JC_10797	17	M	OD	22.61	–	0.46	*TYR* c.1205G>A; p.R402Q *SLC45A2* c.443G>A; p.G148D *SLC45A2* c.665C>A; p.S222Y
JC_11430	15	F	OD	23.40	–	0.28	*TYR* c.575C>A; p.S192Y *TYR* c.1205G>A; p.R402Q *TYR* c.1422_1431del; p.I474Ifr *SLC24A5* c.910A>G; p.K304E
TC_10110‡	40	F	OS	22.99	111,000	0.12	*TYR* c.1205G>A; p.R402Q (hom) *OCA2* c.913C>T; p.R305W *OCA2* c.1256G>A; p.R419Q

* OD, right eye; OS, left eye.
† Subject previously described by Wilk et al.[16]
‡ Subject previously described by Wilk et al.[18]
§ Visual acuity with correction.

approach to estimate the repeatability coefficient from the within-subject standard deviation.[43,44] Intergrader agreement was calculated using the formulae in Bland and Altman,[44] where the replicate assessments from the three graders were used to estimate the mean bias and upper and lower limits of agreement for each pair of graders, along with the 95% confidence intervals for these values. To further explore the effect of the grader on HFL/ONL thickness measurements, linear mixed models with random effects of subject and trial to account for the multiple measurements within subject were used to model the outcomes of HFL and ONL separately for normal and albinism subjects using SAS (SAS Institute Inc., Cary, NC, USA). As the graders segmented the images three times, we also examined the extent by which a learning effect may influence measurement outcomes. The fixed effects of trial, grader, and the interaction of trial and grader were considered statistically significant with a $P < 0.05$.

Results

Subject Demographics

The ages of subjects with albinism ranged from 10 to 69 years old (median, 19.5 years) and 33% were male. The ages of normal controls ranged from 8 to 67 years old (median, 25 years) and 38% were male. There was no significant age difference between the normal and albinism subjects ($P = 0.6251$, Mann-Whitney U test). Axial length was significantly reduced in subjects with albinism (23.26 mm) compared with normal controls (24.24 mm; $P = 0.0354$, unpaired t-test with Welch correction). Additional demographic information for our subjects with albinism is provided in Table 1.

Albinism Genotypes

The oculocutaneous albinism cohort had 18 distinct mutations: nine in *TYR*, five in *OCA2*, two in *SLC45A2*, and two in

Table 2. Intragrader Reliability as Assessed by the Intraclass Correlation Coefficients

	Grader 1			Grader 2			Grader 3		
Layer	**ICC**	**Lower CI**	**Upper CI**	**ICC**	**Lower CI**	**Upper CI**	**ICC**	**Lower CI**	**Upper CI**
Albinism									
HFL+ONL	0.953	0.908	0.999	0.981	0.963	0.999	0.947	0.895	0.998
HFL	0.465	0.118	0.813	0.725	0.498	0.952	0.711	0.475	0.946
ONL	0.882	0.772	0.992	0.876	0.761	0.991	0.875	0.759	0.991
Normal									
HFL+ONL	0.865	0.783	0.948	0.938	0.898	0.978	0.896	0.831	0.961
HFL	0.162	−0.087	0.412	0.114	−0.130	0.359	0.073	−0.165	0.312
ONL	0.870	0.790	0.950	0.902	0.841	0.964	0.613	0.420	0.807

CI, confidence interval.

SLC24A5. One subject, JC_10797, had two different mutations in the *SLC45A2* gene that have not been reported previously to our knowledge (*SLC45A2* c.443G>A, p.Gly148Asp; *SLC45A2* c.665C>A, p.Ser222Tyr). Neither of these variants appear in the gnomAD data (provided in the public domain by gnomad.broadinstitute.org) of over 123,000 exomes and 15,000 genomes (accessed February 28, 2018). The significance of these mutations was also assessed using SIFT, PolyPhen-2, and PROVEAN analysis tools, as previously described.[16] The p.Gly148Asp mutation in *SLC45A2* received the following scores: SIFT, 0; PolyPhen-2, 1.000; and PROVEAN, −6.399, which are classified as damaging, probably damaging, and deleterious, respectively. The p.Ser222Tyr mutation in *SLC45A2* received the following scores: SIFT, 0.19; PolyPhen-2, 0.967; and PROVEAN, −2.142, which are classified as tolerated, probably damaging, and neutral, respectively. Although statistical analysis does not invariably support pathogenicity of the second mutation, it lies between two previously reported mutations within transmembrane domain 6 of the translated MATP protein (*SLC45A2* p.Phe221del[45] and *SLC45A2* p.Cys229Tyr[46]). Thus, it is possible that it represents a hypomorphic polymorphism that, when existing in a compound heterozygous state with a pathogenic mutation, permits a pathogenic phenotype. Additionally, subject JC_11430 had a 10-base pair deletion that induces a frameshift leading to a premature stop codon (*TYR* c.1422_1431del, p.Ile474IlefrTer8). This specific mutation has not been reported previously to our knowledge, but it overlaps with a known 11-base pair deletion (*TYR* c.1423_1433del).[12] This subject also possessed a novel mutation in the *SCL24A5* gene (c.910A>G, p.Lys304Glu), which received the following scores: SIFT, 0.46; PlyPhen-2, 0.546; and PROVEAN, −0.831 (tolerated, possibly damaging, and neutral, respectively). Based on these statistical predictions and the heterozygous state of the mutation, we do not believe this to be a primary contributor to this subject's phenotype. All other mutations in the albinism cohort have been reported previously.

Table 3. Intragrader Repeatability as Assessed by the Within-Subject Standard Deviation*

Layer	Grader 1	Grader 2	Grader 3
Albinism			
HFL+ONL	9.12	6.08	9.91
HFL	17.39	15.62	15.20
ONL	13.75	14.99	14.37
Normal			
HFL+ONL	13.97	9.35	12.32
HFL	10.68	16.11	26.69
ONL	13.05	11.89	25.91

* All values in micrometers.

Intragrader Repeatability of Foveal ONL and HFL Thickness Measurements

Differences in repeatability were observed between graders as well as between the layers (HFL+ONL, HFL, and ONL). The ICC analysis (Table 2) shows that the repeatability of the normal foveal HFL thickness (ICC range, 0.073–0.162) was substantially worse than that of the other layers assessed. This is likely due to the extremely thin subfoveal HFL in normal, where even a one-pixel error results in a large percent change in layer thickness. All graders showed excellent repeatability of foveal HFL+ONL thickness (ICC range, 0.865–0.981), suggesting that the poor HFL repeatability was due to variable segmentation of the posterior HFL boundary (ONL/HFL interface) as opposed to the anterior HFL boundary (ILM or OPL/HFL interface).

As there are known limitations in using ICC when the range of values is particularly small or large,[47] we estimated the intragrader repeatability coefficient by using the approach of Bland and Altman.[43,44] The difference between two measurements for the same subject would be expected to be less than the repeatability coefficient for 95% of pairs of observations. The results in Table 3 provide a similar picture as the ICC analysis, with the foveal HFL+ONL generally having the best repeatability. In addition, we see that grader 3 had markedly worse repeatability of normal ONL and HFL thickness compared with the other two graders, and all three graders performed comparably on the albinism images. This again suggests that the foveal HFL boundary in normal retina is more difficult to assess than in the albinotic retina or simply that small errors in segmentation have a larger relative effect on a thinner layer (normal HFL) than a thicker one (all others). This is further supported by the results of the variance components analysis, where real differences between subjects accounted for 89% of the total variance in albinism foveal ONL measurements, 69% of the total variance in albinism foveal HFL measurements, 85% of the total variance in normal foveal ONL measurements, but only 19% of the total variance in normal foveal HFL measurements.

Intergrader Agreement of Foveal ONL and HFL Thickness Measurements

Table 4 shows the agreement between graders for HFL+ONL, HFL, and ONL thickness measurements for both albinism and normal subjects. Grader 1 and 2 showed excellent agreement, as the 95% confidence intervals for the mean bias included zero for all but one of their thickness measurements (normal

TABLE 4. Intergrader Agreement of Foveal HFL and ONL Thickness Measurements*

	Albinism ($n = 12$)			Normal ($n = 26$)		
Grader	HFL+ONL	HFL	ONL	HFL+ONL	HFL	ONL
Grader 1 and grader 2						
Mean bias† (95% CI)	1.91 (−1.19 to 5.03)	−1.07 (−6.29 to 4.15)	2.98 (−1.63 to 7.60)	−3.31 (−5.80 to −0.82)	−3.16 (−6.98 to 0.65)	−0.14 (−3.98 to 3.68)
Lower LOA‡ (95% CI)	−7.69 (−10.93 to −4.46)	−17.18 (−22.82 to −11.54)	−11.26 (−16.30 to −6.22)	−15.38 (−18.11 to −12.66)	−21.67 (−25.57 to −17.78)	−18.73 (−22.58 to −14.88)
Upper LOA‡ (95% CI)	11.52 (8.29 to 14.76)	15.04 (9.41 to 20.68)	17.23 (12.19 to 22.27)	8.76 (6.04 to 11.48)	15.35 (11.45 to 19.24)	18.44 (14.58 to 22.29)
Grader 1 and grader 3						
Mean bias† (95% CI)	−1.05 (−2.67 to 0.57)	0.34 (−3.42 to 4.11)	−1.40 (−4.79 to 1.99)	0.28 (−1.38 to 1.94)	−7.96 (−10.77 to −5.14)	8.24 (5.57 to 10.91)
Lower LOA‡ (95% CI)	−6.05 (−9.24 to −2.85)	−11.28 (−16.30 to −6.25)	−11.86 (−16.15 to −7.57)	−7.76 (−10.59 to −4.94)	−21.63 (−26.64 to −16.62)	−4.70 (−9.52 to 0.11)
Upper LOA‡ (95% CI)	3.94 (0.75 to 7.13)	11.97 (6.94 to 16.99)	9.07 (4.78 to 13.36)	8.23 (5.50 to 11.15)	5.71 (0.70 to 10.72)	21.18 (16.36 to 26.00)
Grader 2 and grader 3						
Mean bias† (95% CI)	−2.97 (−5.26 to −0.67)	1.41 (−2.25 to 5.08)	−4.38 (−7.56. −1.19)	3.59 (1.55 to 5.63)	−4.79 (−8.75 to −0.84)	8.39 (4.50 to 12.27)
Lower LOA‡ (95% CI)	−10.06 (−12.98 to −7.14)	−9.90 (−14.63 to −5.18)	−14.20 (−18.68 to −9.71)	−6.31 (−8.81 to −3.81)	−23.98 (−28.99 to −18.97)	−10.46 (−15.14 to −5.77)
Upper LOA‡ (95% CI)	4.13 (1.21 to 7.05)	12.73 (8.01 to 17.45)	5.44 (0.95 to 9.93)	13.49 (10.99 to 15.99)	14.39 (9.37 to 19.39)	27.23 (22.55 to 31.92)

* All values in micrometers.

† 95% confidence intervals (CI) on the mean bias is estimated as $\pm$ t standard errors, using $n-1$ df to find the appropriate point of the t distribution.

‡ Upper and lower limits of agreement (LOA) calculated per equation 5.3 in Bland and Altman.[44] Variance of the LOA calculated per equation 5.10 in Bland and Altman,[44] using $m_x = m_y = 3$. Standard error is the square root of the variance, and the 95% CIs on the LOA were estimated as ± 1.96 (standard error).

HFL+ONL). Worse agreement was seen for the normal ONL and HFL data between grader 1 and grader 3, although the 95% confidence intervals for all albinism measures again included zero (as with the grader 1/grader 2 comparison). The worst agreement was seen when comparing grader 2 and grader 3, where all layers except the albinism HFL showed significant bias between the two graders, with the mean bias ranging from −2.97 to 8.39 μm.

Returning to the linear mixed models, the fixed effects of grader and trial were significant, as well as the grader and trial interaction effect. This may indicate a learning effect over repeated segmentation of images by the graders. Adding a learning effect to the model was significant for normal ONL and HFL for all three graders, although no significant learning effect was seen for albinism ONL and HFL measures. These model results are shown in Figure 3. The reciprocal slope of the normal ONL data relative to the normal HFL data is consistent with a shifting of the ONL/HFL boundary as opposed to any changes in the segmentation of the posterior ONL boundary (ELM) or the anterior HFL boundary (ILM or HFL/OPL).

Foveal ONL and HFL Thickness in Albinism

To compare the ONL and HFL between normal and albinism subjects, we used the average thickness values from all nine trials. Figure 4 shows a summary of the combined HFL+ONL, HFL, and ONL thickness data from the fovea for normal and albinism subjects. There was no difference in foveal HFL+ONL thickness between the albinism subjects and normal controls ($P = 0.3169$, t = 1.028, degrees of freedom [df] = 18.72; unpaired t-test with Welch correction). Looking at the ONL and HFL separately, we find that the ONL layer at the incipient fovea in our subjects with albinism was significantly thinner than in our normal controls ($P < 0.0001$, t = 5.22, $df = 19.49$; unpaired t-test with Welch correction), whereas the HFL layer was significantly thicker ($P < 0.0001$, t = 12.01, $df = 12.63$; unpaired t-test with Welch correction). As with other retinal features, there was overlap between the two populations (Fig. 4).

ONL and HFL Topography in Albinism

Given the observed difference in foveal ONL and HFL layer thickness, we were interested to see if there was general thinning or if there was simply a topographical "redistribution" within these layers. The ONL and HFL thickness was assessed within ±2 mm of the fovea (Fig. 5). The total AUC of the ONL and HFL was also calculated to assess whether the overall quantity of ONL and HFL across the fovea was altered between the two populations as a sequela of foveal hypoplasia evident in subjects with albinism. The HFL remained thicker in albinism than normal until about 0.4-mm nasal or temporal, after which HFL was thicker in the normal controls (Fig. 5A). The total AUC of the HFL in subjects with albinism did not significantly differ from the total AUC of the HFL in normal controls ($P = 0.1560$, t = 1.479, $df = 18.29$; unpaired t-test with Welch correction). Both the albinism subjects and normal controls showed an increased ONL thickness at the fovea relative to the parafovea, although the increase was much more pronounced in the normal controls (Fig. 5B). Beyond about 0.5-mm nasal or temporal, the albinism subjects and normal controls had similar ONL thickness (Fig. 5B). The total AUC of the ONL in subjects with albinism was not significantly different from that of normal controls ($P = 0.1048$, t = 1.691, $df = 22.25$; unpaired t-test with Welch correction).

The relative contribution of the HFL to the HFL+ONL varied between subjects and between the two patient groups (Fig. 5C). On average, HFL thickness at the incipient fovea in subjects with albinism comprised 42.8% of the measured

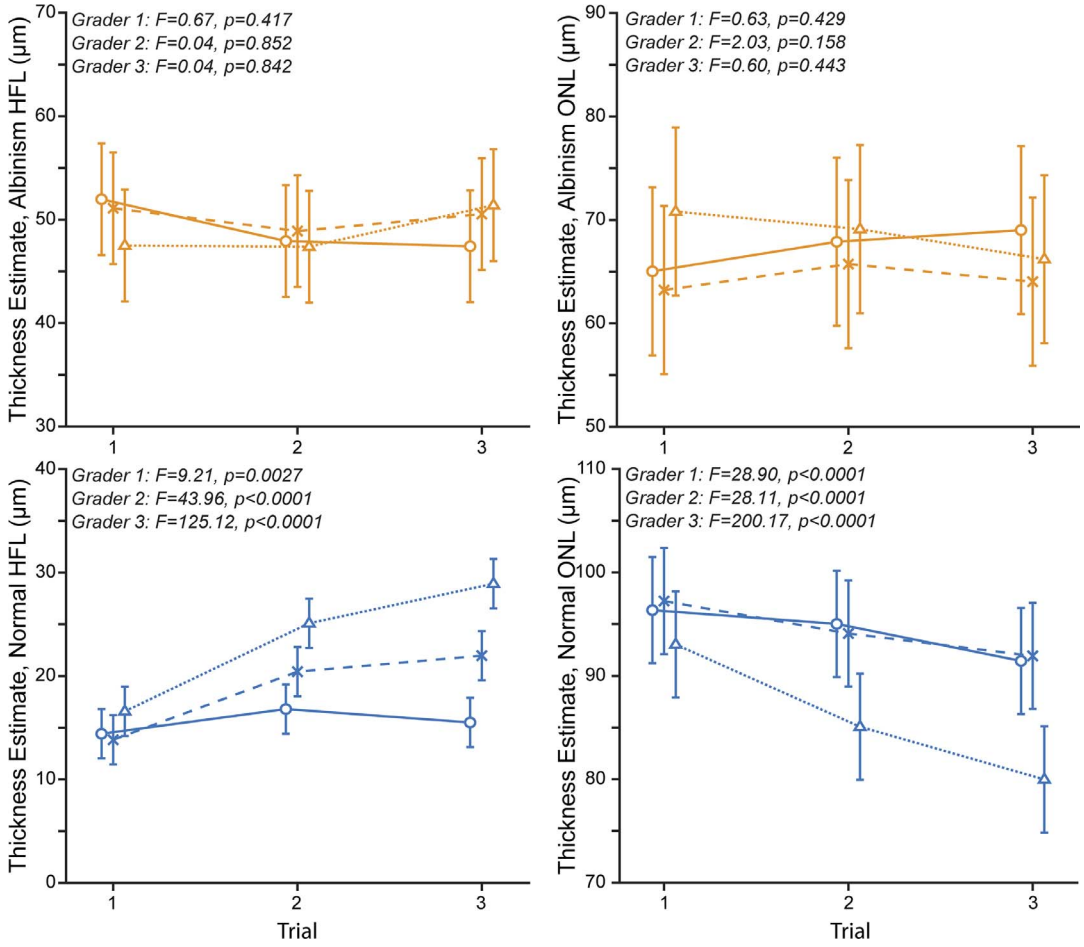

Figure 3. Model-based estimates for each grader and trial are presented along with standard errors. These plots illustrate the learning over time effect for ONL and HFL for both the normal and albinism subjects. *Open circles* are from grader 1, *crosses* are from grader 2, and *open triangles* are from grader 3. F statistics for each grader are provided in each panel, along with the corresponding *P* value. No significant learning effect was seen in the albinism data, whereas significant learning effects were seen for the ONL and HFL measurements from normal. Note that the range on the *y*-axis is the same for each plot in magnitude but shifted to be roughly centered on the data for each metric. This was done to focus on differences between graders and trials and not necessarily to facilitate comparisons of the absolute value of the HFL or ONL thicknesses between albinism and normal (which is detailed in Fig. 4).

HFL+ONL thickness (range, 29.8%–50.2%). In comparison, the HFL comprised only 17.5% of the measured HFL+ONL thickness (range, 11.4%–24.8%) at the fovea in our normal controls. Beyond about 0.5 mm from the fovea, the HFL comprised more than 50% of the measured HFL+ONL thickness on average for both the albinism and normal subjects. The data for our normal controls are consistent with previous results.[38]

Although our quantitative analyses were restricted to horizontal B-scans, we did examine en face images extracted from the volumetric scans for two subjects. The en face images (acquired using a 20-µm-thick contour based on the ellipsoid zone and positioned at the depth of the HFL) reveal a series of concentric rings around the location of the incipient fovea at the level of the HFL (Fig. 6). This can be seen in the B-scans, where the parafoveal HFL is not a uniform layer, but alternating hypo- and hyperreflective vertical bands/blobs (Fig. 6). The series of concentric rings was not visible at any other level of the retina. Prior literature has reported a similar phenomenon observed in subjects with foveal hypoplasia when using infrared reflectance as well as scanning laser polarimetry with variable corneal compensation (with Zeiss GDx VCC retinal scanner).[48] Although the authors attributed the presence of this "concentric macular ring sign" as the result of the radially symmetric orientation of the HFL and RNFL around the incipient fovea, our data suggest that the concentric rings present in foveal hypoplasia occur exclusively at the level of the HFL. It remains unclear exactly how the HFL orientation differs in albinism and other conditions with foveal hypoplasia to give rise to this distinct patterning.

Foveal ONL Thickness and Peak Cone Density in Albinism

Images of the cone mosaics were available for 10 of the 12 subjects with albinism. Cone density ranged from 71,600 to 124,100 cones/mm^2 (Table 1). We found a strong positive correlation between peak cone density and ONL thickness at the foveal center in our subjects with albinism (Spearman r = 0.8061, $P = 0.0072$, $df = 8$), as shown in Figure 7.

Discussion

Implications for Current Models of Foveal Development

Our data demonstrate that a robust HFL can exist in the absence of a foveal pit. This supports a relative lateral

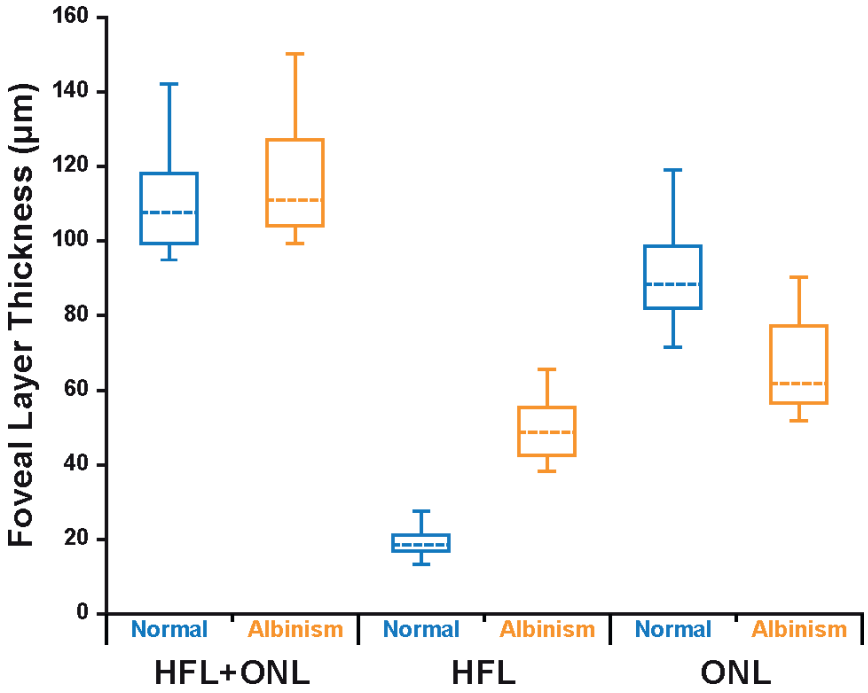

Figure 4. Abnormal foveal ONL and HFL thickness in albinism. Shown are the median thickness values (*dashed horizontal lines*) for both the albinism group (*orange*) and the normal controls (*blue*). The 25th and 75th quartiles are represented by the *rectangles*, and the *error bars* extend to the minimum and maximum values for each dataset. Total HFL+ONL thickness was not significantly different between albinism and controls ($P = 0.3169$). Foveal HFL thickness was thicker in albinism than in normal controls ($P < 0.0001$), and foveal ONL thickness was thinner in albinism than in normal controls ($P < 0.0001$).

displacement of bipolar neurons with respect to their cone photoreceptor inputs in subjects with albinism. This is consistent with prior studies showing that cone packing at the fovea can occur in the absence of a foveal pit.[2,14,16,19] Thus, at least at some level, the process of foveal cone packing occurs independently of the processes guiding the displacement of the inner retinal layers away from the fovea. Regardless of their dependence, these processes likely both contribute to building a foveal region that supports high visual acuity, although previous data showed no correlation between peak foveal cone density and visual acuity.[16] This discrepancy could be explained by the recent observation that the 1:1 cone to ganglion cell connectivity can be disrupted in retinas with foveal hypoplasia (Dacey DM, *IOVS* 2018;59:ARVO E-Abstract 14). Although there is foveal cone packing in albinism, it does appear to be generally lower than in normal[16]; thus, the prominent foveal HFL in these subjects is somewhat paradoxical. Altered size or position of Müller glia[33] or increased size of the cone axons in albinism may contribute to the measured foveal HFL in albinism, although this could be addressed by assessing donor eyes in a future study.

In the present study, all but one of the albinism subjects had visual acuity better than 20/63 (logMAR, 0.50) and 4 of 12 were 20/25 (logMAR, 0.10) or better. Thus, it was not possible to examine any relationship between HFL/ONL topography and visual acuity. Future studies should examine foveal anatomy across a wider phenotypic range of albinism, as well as examine possible genotype-dependent differences (which was not possible here due to the small number of subjects). In addition, assessing ganglion cell topography in relation to HFL and ONL topography would capture important postreceptoral aspects of foveal development and such data could facilitate further modeling of structure-function relationships in albinism.[49]

Assessing Intra- and Intergrader Variability in Manual Segmentation of D-OCT

Modest inter- and intragrader variability in manual measurements is not unique to our study and has been reported in other studies.[50–52] Other studies have shown improved repeatability and reproducibility with the use of computer-aided manual segmentation procedures.[53] However, until automated algorithms are developed for D-OCT images, manual segmentation will continue to be important when assessing HFL and ONL topography. Thus, it is important that studies provide a transparent presentation of the behavior of their grader(s). As demonstrated in our study, grader effects (including learning effects) can influence resultant ONL and HFL measurements in D-OCT images from both the normal and albinism retina. More training on D-OCT segmentation may help reduce performance variability within and between graders. For measurements of HFL to become routine in a clinical or reading center environment, automated segmentation methods will likely be required to overcome the intergrader variability in performance exhibited in our study. To this end, our manual segmentation results may help inform the development and validation of such algorithms in future studies.

Limitations

Our analysis of ONL and HFL thickness may be limited by the sequential acquisition of OCT images. As OCT images were acquired sequentially rather than simultaneously, measurements of the HFL and ONL can be vulnerable to alterations in fixation during image acquisition. In our study, we sought to minimize this limitation and verify axial and lateral registration by comparing the ILM and retinal pigment epithelium contours and the choroidal vessels in all three scans. A functionality in

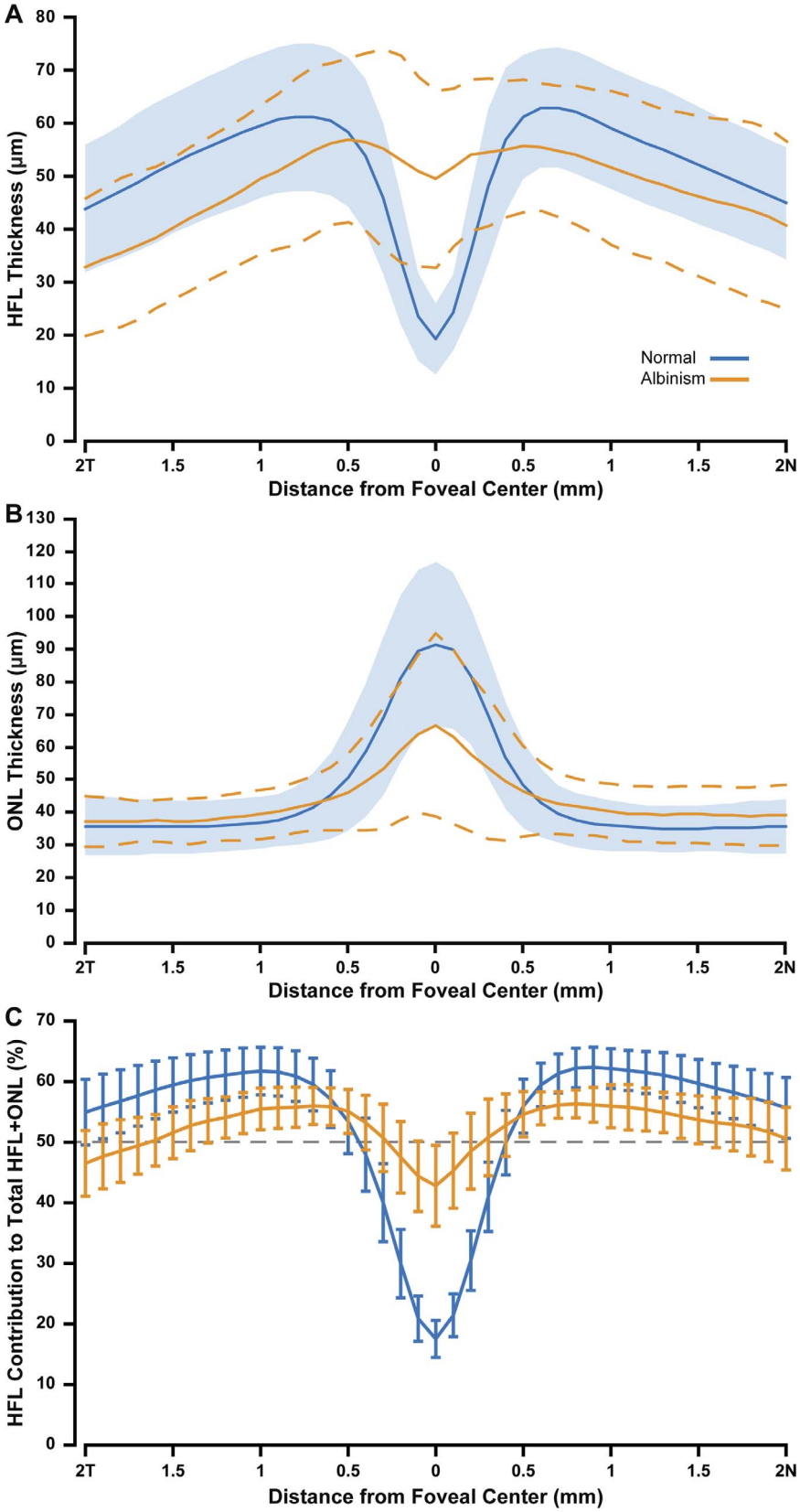

Figure 5. Assessing ONL and HFL topography. Shown are plots of HFL thickness (**A**) and ONL thickness (**B**) for both albinism (*orange*) and normal controls (*blue*). The *solid lines* represent the average layer thickness in albinism and normal controls. *Dashed orange lines* represent two standard deviations above and below the average layer thickness in albinism, and the *blue shaded area* represents two standard deviations above and below the average retinal thickness in our normal controls. (**C**) The percent contribution of the HFL to the total HFL+ONL thickness across the horizontal line scan for both groups of subjects (*error bars* represent one standard deviation above and below the mean; *dashed gray line* represents 50% HFL contribution).

Investigative Ophthalmology & Visual Science

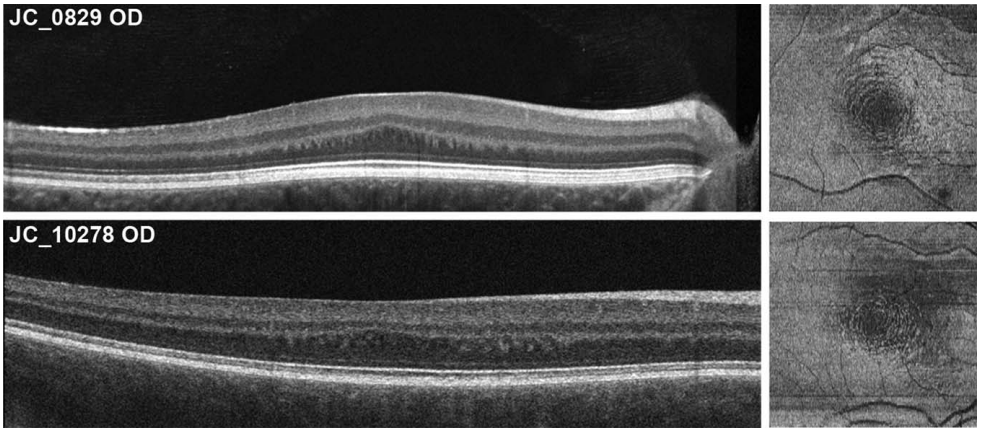

FIGURE 6. En face OCT image, alongside their respective B-scan, displaying the concentric nature of the HFL in two of our subjects with albinism (JC_0829 and JC_10278). Volumetric OCT scans were analyzed using the "en face analysis" setting of the Cirrus software. A 20-μm-thick ellipsoid zone-based contour positioned at the depth of the HFL was used to obtain two en face images at differing levels of the HFL. They were subsequently stacked on ImageJ by using the "images to stack" function and then averaged using the Z-project function to obtain the final en face images.

the OCT software in the future that would allow for three simultaneous images to be taken with varying pupil entry positions and merge the images together may also address this limitation. An additional limitation to our study is the difference in axial length in our two study groups, although for our AUC analyses, we did correct the lateral scale of each D-OCT triad for magnification differences due to axial length differences prior to analysis. Prior studies have demonstrated that the greater axial length in myopes is associated with thinner peripheral retina, although there are mixed results on its effect on foveal retinal thickness measurements.[54,55] Regardless of this limitation, our study demonstrates clear differences in HFL and ONL topography between the two populations, and axial length is unlikely to account for the extent of topographic differences seen in our study. Although the longer axial length of our normal subjects may explain the slightly (although nonsignificantly) reduced HFL+ONL thickness in normal compared to albinism retinae (Fig. 4), the pronounced differences in the HFL contribution to the foveal HFL+ONL thickness between the two groups (Figs. 4, 5) are unlikely to be explained by axial length effects on total retinal thickness.

Another limitation to this study was the low number of subjects with albinism with adequate quality imaging. Although we have shown that D-OCT is feasible in this population, we were unable to succeed in imaging more subjects due to the high prevalence of nystagmus in albinism. Beyond the low statistical power in our analyses, the conclusions may be limited, as our subjects may not capture the full range of albinism phenotypes (as stated above). In addition, we only assessed HFL and ONL thickness along horizontal cross sections of the fovea. We did not analyze HFL and ONL thickness along the vertical cross sections of the fovea nor did we consider the concentric nature of the HFL (Fig. 6). Anisotropy of the ONL and HFL layers may be important when examining their relationship to other anatomic landmarks associated with the fovea (i.e., foveal avascular zone, pit morphology, and cone topography).

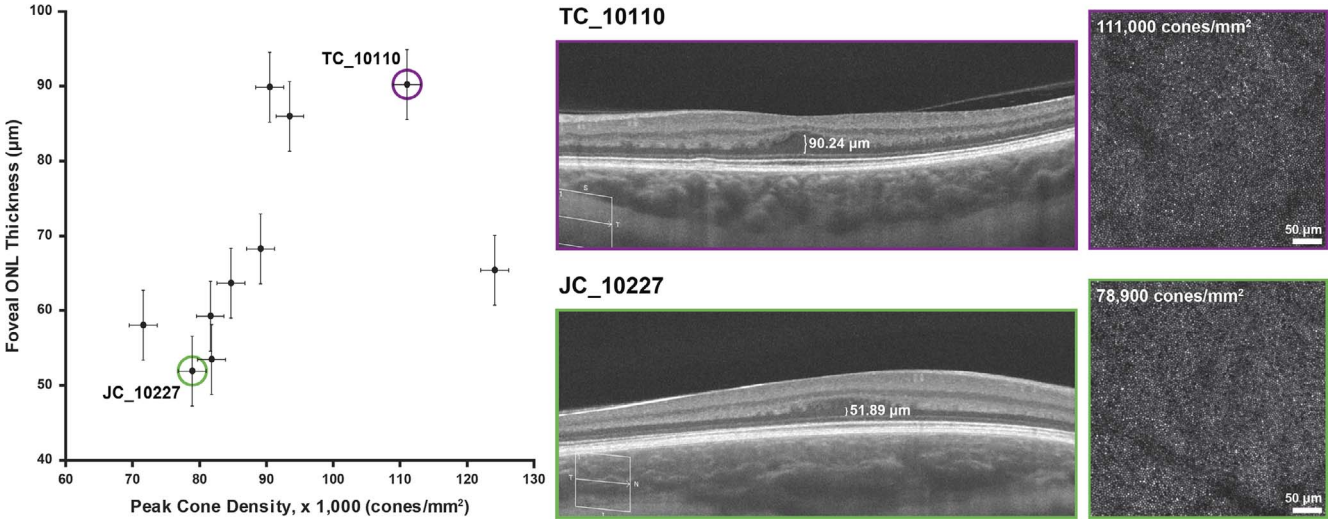

FIGURE 7. Relationship between foveal ONL thickness and peak cone density in albinism demonstrates a strong positive correlation (Spearman r = 0.8061, $P = 0.0072$). Shown on the right are D-OCT images and AOSLO images of the foveal cone mosaic for two subjects with relatively high (TC_10110) and low (JC_10227) cone densities. *Vertical error bars* represent standard error, and the *horizontal error bars* represent measurement error and are based on prior literature on AOSLO cone density measurements.[42]

Examining OCT-Based Biomarkers of Foveal Cone Packing

Because OCT technology is readily available and the ONL is primarily comprised of photoreceptor cell bodies, ONL thickness has been used to provide a convenient and noninvasive measure of photoreceptor "health" when studying retinal degenerative diseases.[20–23] In our study, we found a positive correlation between "true" foveal ONL thickness and peak cone density in subjects with albinism. This relationship has been explored in both normal subjects as well as in subjects with retinal degenerative diseases in prior literature.[11,56–58] Menghini et al.[57] found a correlation between ONL thickness and cone density in normal eyes at varying retinal eccentricities. However, the authors found that retinal eccentricity was a more important predictor of cone density than ONL thickness. Additionally, they did not explore the relationship between foveal ONL thickness and peak cone density. Langlo et al.[23] did not find a correlation between foveal ONL thickness and cone density in subjects with achromatopsia; however, the authors did not use D-OCT to delineate the ONL from the HFL, precluding accurate analysis of this relationship in their subjects. Correlating other OCT image findings with peak cone density has also been reported in prior literature. Wilk et al.[18] found a strong correlation between outer segment length and peak cone density values in subjects with albinism. However, in their normal controls, this correlation no longer existed. This was largely attributed to the underestimation of peak cone density in AOSLO images when compared with those reported in histology. Overall, outer segment length appears to correlate better with cone density values than foveal ONL thickness measurements obtained from D-OCT. This is likely because the signals in confocal AOSLO images are derived from the photoreceptor outer segments. We did not measure outer segment length in the present study due to limited axial resolution of the Cirrus OCT used here compared with the Bioptigen OCT used in the Wilk et al.[18] study. In addition, only line scans were available from these subjects, obviating the ability to confirm measurement at the location of maximum foveal depression and/or outer segment lengthening. Nevertheless, D-OCT is a robust method with which to assess foveal ONL thickness, which can be exploited in future studies of foveal cone specialization.

Toward a Quantitative Classification of Foveal Hypoplasia

In 2011, Thomas et al.[4] proposed a valuable qualitative grading system for assessing the extent of foveal hypoplasia in several diseases that classically present with arrested foveal development. As we have demonstrated here and previously,[16,18,23] OCT enables the extraction of various quantitative parameters regarding foveal anatomy. Such data could help refine the application and sensitivity of such grading schemes. For example, based on the observation that some patients with albinism can actually have foveal pits that are within normal limits with respect to their size, Wilk et al.[16] proposed including quantitative data on foveal pit morphology to stratify individuals with grade 1 hypoplasia per the Thomas et al.[4] scheme. Beyond the pit, the two elements of the Thomas et al.[4] grading scheme that directly assess photoreceptor specialization at the fovea are outer segment lengthening and ONL widening. Wilk et al.[18] showed that outer segment length in albinism is a reasonable surrogate for measuring the degree of foveal cone packing, and outer segment length values in albinism range from 26.3 to 41.5 μm (normal range, 40.2–54.5 μm).[18] Thus it may be that rather than a binary "presence" or "absence" of outer segment lengthening, foveal grading schemes could use quantitative data on outer segment length to more objectively classify a given retina within grades 1 and 2. Likewise, as presented in the current study, the ability to measure the increased ONL thickness evident at the fovea allows one to specify the extent of ONL "widening," not just whether it is present or absent. This could be used to refine grades 1, 2, and 3, as they all include "presence of ONL widening" as a characteristic feature. The present study introduces an additional anatomic factor besides the original four proposed by Thomas et al.,[4] namely the HFL. The presence of the HFL is a signature of relative lateral displacement between inner retinal neurons and their cone inputs. Thus, it may be useful either alone or in combination with the ONL thickness to revise grades 1, 2, and/or 3 in the Thomas et al.[4] scheme. Larger datasets incorporating all the abovementioned quantitative measures are needed to facilitate the development and validation of any new grading scheme. Such grading may be of interest when looking to correlate the severity of hypoplasia with functional measures of vision in albinism and other populations. Additionally, macular pigment distribution has been associated with visual outcomes in both eyes with and without ocular pathology.[59–61] As the HFL is where the macular pigment resides, assessing macular pigment distribution may provide yet another method to quantify foveal maturity in albinism and other disorders, as was recently demonstrated by Sauer et al.[62]

Conclusions

In conclusion, we demonstrate significant differences in ONL and HFL thickness and topography between subjects with normal vision and those with albinism. As the HFL comprises a variable percentage of the HFL+ONL thickness (colloquially referred to as the ONL in most published OCT studies), both across subjects and retinal location, estimates of ONL thickness that do not subtract out the HFL contribution are inaccurate. The observation of a robust HFL in albinism subjects with foveal hypoplasia suggests that increased foveal cone packing drives the formation of Henle fibers more so than the lateral displacement of inner retina.

Acknowledgments

Presented at the annual meeting of the Association for Research in Vision and Ophthalmology, Baltimore, Maryland, United States, 2017.

The authors thank Erin Curran, Brian Higgins, Alex Salmon, Phyllis Summerfelt, and Maureen Tuffnell and for their contributions to this work. The authors also thank Elizabeth McPherson, Harold Ye, Jennifer Anderson, and Jeff Joyce for help with the sequencing and genetic analysis.

Supported by the National Institutes of Health under award numbers K12EY017269, TL1TR001437, T32GM080202, P30EY001931, and R01EY024969. This project was supported in part by the National Center for Advancing Translational Sciences, National Institutes of Health, through grant number UL1TR001436. This investigation was conducted in part in a facility constructed with support from the Research Facilities Improvement Program, grant C06RR016511 from the National Center for Research Resources, National Institutes of Health. The content is solely the responsibility of the authors and does not necessarily represent the official views of the National Institutes of Health. Additional support from the Thomas M. Aaberg, Sr., Retina Research Fund; Vision for Tomorrow; and Research to Prevent Blindness, Inc. (MCW, University of Minnesota).

Disclosure: **D.J. Lee**, None; **E.N. Woertz**, None; **A. Visotcky**, None; **M.A. Wilk**, None; **H. Heitkotter**, None; **R.E. Linderman**, None; **S. Tarima**, None; **C.G. Summers**, None; **B.P. Brooks**, None; **M.H. Brilliant**, None; **B.J. Antony**, IBM (E); **B.J. Lujan**,

Genentech/Roche (F), Optovue (S), Zeiss (S), BioTime/CellCure (C), P; **J. Carroll**, Optovue (F), P

References

1. Yuodelis C, Hendrickson A. A qualitative and quantitative analysis of the human fovea during development. *Vision Res*. 1986;26:847–855.
2. Provis JM, Dubis AM, Maddess T, Carroll J. Adaptation of the central retina for high acuity vision: cones, the fovea, and the avascular zone. *Prog Retin Eye Res*. 2013;35:63–81.
3. Summers CG. Vision in albinism. *Trans Am Ophthalmol Soc*. 1996;94:1095–1155.
4. Thomas MG, Kumar A, Mohammad S, et al. Structural grading of foveal hypoplasia using spectral-domain optical coherence tomography: a predictor of visual acuity? *Ophthalmology*. 2011;118:1653–1660.
5. Cunha-Vaz J, Ribeiro L, Lobo C. Phenotypes and biomarkers of diabetic retinopathy. *Prog Retin Eye Res*. 2014;41:90–111.
6. Hendrickson AE, Yuodelis C. The morphological development of the human fovea. *Ophthalmology*. 1984;91:603–612.
7. Hendrickson A, Provis J. Comparison of development of the primate fovea centralis with peripheral retina. In: Sernagor E, Eglen S, Harris B, Wong R, eds. *Retinal Development*. Cambridge: Cambridge University Press; 2006.
8. Dubis AM, Costakos DM, Subramaniam CD, et al. Evaluation of normal human foveal development using optical coherence tomography and histologic examination. *Arch Ophthalmol*. 2012;130:1291–1300.
9. Vinekar A, Mangalesh S, Jayadev C, Maldonado R, Bauer N, Toth C. Retinal imaging of infants on spectral domain optical coherence tomography. *Biomed Res Int*. 2015;2015:782420.
10. Lee H, Proudlock FA, Gottlob I. Pediatric optical coherence tomography in clinical practice–recent progress. *Invest Ophthalmol Vis Sci*. 2016;57:OCT69–OCT79.
11. Sjöstrand J, Rosén R, Nilsson M, Popovic Z. Arrested foveal development in preterm eyes: Thickening of the outer nuclear layer and structural redistribution within the fovea. *Invest Ophthalmol Vis Sci*. 2017;58:4948–4958.
12. King RA, Pietsch J, Fryer JP, et al. *Tyrosinase* gene mutations in oculocutaneous albinism 1 (OCA1): definition of the phenotype. *Hum Genet*. 2003;113:502–513.
13. Chong GT, Farsiu S, Freedman SF, et al. Abnormal foveal morphology in ocular albinism imaged with spectral-domain optical coherence tomography. *Arch Ophthalmol*. 2009;127:37–44.
14. McAllister JT, Dubis AM, Tait DM, et al. Arrested development: high-resolution imaging of foveal morphology in albinism. *Vision Res*. 2010;50:810–817.
15. Seo JH, Yu YS, Kim JH, Choung HK, Heo JW, Kim SJ. Correlation of visual acuity with foveal hypoplasia grading by optical coherence tomography in albinism. *Ophthalmology*. 2007;114:1547–1551.
16. Wilk MA, McAllister JT, Cooper RF, et al. Relationship between foveal cone specialization and pit morphology in albinism. *Invest Ophthalmol Vis Sci*. 2014;55:4186–4198.
17. McCafferty BK, Wilk MA, McAllister JT, et al. Clinical insights into foveal morphology in albinism. *J Pediatr Ophthalmol Strabismus*. 2015;52:167–172.
18. Wilk MA, Wilk BM, Langlo CS, Cooper RF, Carroll J. Evaluating outer segment length as a surrogate measure of peak foveal cone density. *Vision Res*. 2017;130:57–66.
19. Marmor MF, Choi SS, Zawadzki RJ, Werner JS. Visual insignificance of the foveal pit: Reassessment of foveal hypoplasia as fovea plana. *Arch Ophthalmol*. 2008;126:907–913.
20. Cideciyan AV, Jacobson SG, Beltran WA, et al. Human retinal gene therapy for Leber congenital amaurosis shows advancing retinal degeneration despite enduring visual improvement. *Proc Natl Acad Sci U S A*. 2013;110:E517–E525.
21. Ramachandran R, Zhou L, Locke KG, Birch DG, Hood DC. A comparison of methods for tracking progression in X-linked retinitis pigmentosa using frequency domain OCT. *Trans Vis Sci Tech*. 2013;2(7):5.
22. Huang WC, Cideciyan AV, Roman AJ, et al. Inner and outer retinal changes in retinal degenerations associated with ABCA4 mutations. *Invest Ophthalmol Vis Sci*. 2014;55:1810–1822.
23. Langlo CS, Patterson EJ, Higgins BP, et al. Residual foveal cone structure in *CNGB3*-associated achromatopsia. *Invest Ophthalmol Vis Sci*. 2016;57:3984–3995.
24. Putnam NM, Hammer DX, Zhang Y, Merino D, Roorda A. Modeling the foveal cone mosaic imaged with adaptive optics scanning laser ophthalmoscopy. *Opt Express*. 2010;18:24902–24916.
25. Rossi EA, Roorda A. The relationship between visual resolution and cone spacing in the human fovea. *Nat Neurosci*. 2010;13:156–157.
26. Zhang T, Godara P, Blancob ER, et al. Variability in human cone topography assessed by adaptive optics scanning laser ophthalmoscopy. *Am J Ophthalmol*. 2015;160:290–300.
27. Wilk MA, Dubis AM, Cooper RF, Summerfelt P, Dubra A, Carroll J. Assessing the spatial relationship between fixation and foveal specializations. *Vision Res*. 2017;132:53–61.
28. Milam AH, Li ZY, Fariss RN. Histopathology of the human retina in retinitis pigmentosa. *Prog Retin Eye Res*. 1998;17:175–205.
29. Wang W, Lee SJ, Scott PA, et al. Two-step reactivation of dormant cones in retinitis pigmentosa. *Cell Reports*. 2016;15:372–385.
30. Kaplan HJ, Wang W, Dean DC. Restoration of cone photoreceptor function in retinitis pigmentosa. *Trans Vis Sci Tech*. 2017;6(5):5.
31. Lujan BJ, Roorda A, Knighton RW, Carroll J. Revealing Henle's fiber layer using spectral domain optical coherence tomography. *Invest Ophthalmol Vis Sci*. 2011;52:1486–1492.
32. Otani T, Yamaguchi Y, Kishi S. Improved visualization of Henle fiber layer by changing the measurement beam angle on optical coherence tomography. *Retina*. 2011;31:497–501.
33. Syrbe S, Kuhrt H, Gartner U, et al. Muller glial cells of the primate foveola: an electron microscopical study. *Exp Eye Res*. 2017;167:110–117.
34. Anger EM, Unterhuber A, Hermann B, et al. Ultrahigh resolution optical coherence tomography of the monkey fovea. Identification of retinal sublayers by correlation with semithin histology sections. *Exp Eye Res*. 2004;78:1117–1125.
35. Christensen UC, Kroyer K, Thomadsen J, Jorgensen TM, la Cour M, Sander B. Normative data of outer photoreceptor layer thickness obtained by software image enhancing based on Stratus optical coherence tomography. *Br J Ophthalmol*. 2008;82:800–805.
36. Rha J, Dubis AM, Wagner-Schuman M, et al. Spectral domain optical coherence tomography and adaptive optics: imaging photoreceptor layer morphology to interpret preclinical phenotypes. *Adv Exp Med Biol*. 2010;664:309–316.
37. Spaide RF. Outer retinal atrophy after regression of subretinal drusenoid deposits as a newly recognized form of late age-related macular degeneration. *Retina*. 2013;33:1800–1808.
38. Lujan BJ, Roorda A, Croskrey JA, et al. Directional optical coherence tomography provides accurate outer nuclear layer and Henle fiber layer measurements. *Retina*. 2015;35:1511–1520.

Investigative Ophthalmology & Visual Science

39. Makhijani VS, Roorda A, Bayabo JK, Tong KK, Rivera-Carpio CA, Lujan BJ. Chromatic visualization of reflectivity variance within hybridized directional OCT images. *Proceedings of SPIE*. Bellingham, WA: SPIE; 2013:8571:857105.
40. Schneider CA, Rasband WS, Eliceiri KW. NIH image to ImageJ: 25 years of image analysis. *Nat Methods*. 2012;9:671–675.
41. Dubra A, Sulai Y, Norris JL, et al. Noninvasive imaging of the human rod photoreceptor mosaic using a confocal adaptive optics scanning ophthalmoscope. *Biomed Opt Express*. 2011; 2:1864–1876.
42. Garrioch R, Langlo C, Dubis AM, Cooper RF, Dubra A, Carroll J. Repeatability of in vivo parafoveal cone density and spacing measurements. *Optom Vis Sci*. 2012;89:632–643.
43. Bland JM, Altman DG. Statistics notes: Measurement error. *Br Med J* (*Clin Res Ed*). 1996;313:744.
44. Bland JM, Altman DG. Measuring agreement in method comparison studies. *Stat Methods Med Res*. 1999;8:135–160.
45. Rundshagen U, Zühlke C, Opitz S, Schwinger E, Käsmann-Kellner B. Mutations in the MATP gene in five German patients affected by oculocutaneous albinism type 4. *Hum Mutat*. 2004;23:106–110.
46. Inagaki K, Suzuki T, Ito S, et al. Oculocutaneous albinism type 4: Six novel mutations in the membrane-associated transporter protein gene and their phenotypes. *Pigment Cell Res*. 2006;19:451–453.
47. Bland JM, Altman DG. A note on the use of the intraclass correlation coefficient in the evaluation of agreement between two methods of measurement. *Comput Biol Med*. 1990;20:337–340.
48. Cornish KS, Reddy AR, McBain VA. Concentric macular rings sign in patients with foveal hypoplasia. *JAMA Ophthalmol*. 2014;132:1084–1088.
49. von dem Hagen EA, Houston GC, Hoffmann MB, Jeffery G, Morland AB. Retinal abnormalities in human albinism translate into a reduction of grey matter in the occipital cortex. *Eur J Neurosci*. 2005;22:2475–2480.
50. Kwon YH, Adix M, Zimmerman MB, et al. Variance owing to observer, repeat imaging, and fundus camera type on cup-to-disc ratio estimates by stereo planimetry. *J Glaucoma*. 2009; 18:305–310.
51. Abozaid MA, Langlo CS, Dubis AM, Michaelides M, Tarima S, Reliability Carroll J. and repeatability of cone density measurements in patients with congenital achromatopsia. *Adv Exp Med Biol*. 2016;854:277–283.
52. Tanna P, Kasilian M, Strauss R, et al. Reliability and repeatability of cone density measurements in patients with Stargardt disease and RPGR-associated retinopathy. *Invest Ophthalmol Vis Sci*. 2017;58:3608–3615.
53. Hood DC, Cho J, Raza AS, Dale EA, Wang M. Reliability of a computer-aided manual procedure for segmenting optical coherence tomography scans. *Optom Vis Sci*. 2011;88:113–123.
54. Song AP, Wu X, Wang J, Liu W, Sun Y, Yu T. Measurement of retinal thickness in macular region of high myopic eyes using spectral domain OCT. *Int J Ophthalmol*. 2014;7:122–127.
55. Jonas JB, Xu L, Wei WB, et al. Retinal thickness and axial length. *Invest Ophthalmol Vis Sci*. 2016;57:1791–1797.
56. Chui TY, Song H, Clark CA, Papay JA, Burns SA, Elsner AE. Cone photoreceptor packing density and the outer nuclear layer thickness in healthy subjects. *Invest Ophthalmol Vis Sci*. 2012;53:3545–3553.
57. Menghini M, Lujan BJ, Zayit-Soudry S, et al. Correlation of outer nuclear layer thickness with cone density values in patients with retinitis pigmentosa and healthy subjects. *Invest Ophthalmol Vis Sci*. 2014;56:372–381.
58. Nakamura T, Ueda-Consolvo T, Oiwake T, Hayashi A. Correlation between outer retinal layer thickness and cone density in patients with resolved central serous chorioretinopathy. *Graefes Arch Clin Exp Ophthalmol*. 2016;254:2347–2354.
59. Hammond BR, Wooten BR, Snodderly DM. Preservation of visual sensitivity of older subjects: association with macular pigment density. *Invest Ophthalmol Vis Sci*. 1998;39:397–406.
60. Wooten BR, Hammond BR. Macular pigment: influence on visual acuity and visibility. *Prog Retin Eye Res*. 2002;21:225–240.
61. Puell MC, Palomo-Alvarez C, Barrio AR, Gómez-Sanz FJ, Pérez-Carrasco MJ. Relationship between macular pigment and visual acuity in eyes with early age-related macular degeneration. *Acta Ophthalmol*. 2013;91:298–303.
62. Sauer L, Andersen KM, Li B, Gensure RH, Hammer M, Bernstein PS. Fluorescence lifetime imaging ophthalmoscopy (FLIO) of macular pigment. *Invest Ophthalmol Vis Sci*. 2018; 59:3094–3103.

Supplementary Materials

Supplementary Video S1. Registered D-OCT images from a normal control. Frame sequence shows an image acquired with pupil entry offset in the nasal direction, followed by the average of the images acquired under the three different pupil entry positions along with the retinal layer segmentation, followed by the image acquired with pupil entry offset in the temporal direction, and then again the averaged image with layer segmentation markings.

Supplementary Video S2. Registered D-OCT images from a subject with albinism. Frame sequence shows an image acquired with pupil entry offset in the nasal direction, followed by the average of the images acquired under the three different pupil entry positions along with the retinal layer segmentation, followed by the image acquired with pupil entry offset in the temporal direction, and then again the averaged image with layer segmentation markings.

Investigative Ophthalmology & Visual Science